

# Wavelength limits on isobaricity of perturbations in a thermally unstable radiatively cooling medium

I. G. Kovalenko

*Department of Physics, Volgograd State University, Volgograd 400062, Russia*

Yu. A. Shchekinov

*Department of Physics, Rostov State University, Rostov on Don 344090, Russia*

(September 10, 2018)

Nonlinear evolution of one-dimensional planar perturbations in an optically thin radiatively cooling medium in the long-wavelength limit is studied numerically. The accepted cooling function generates in thermal equilibrium a bistable equation of state  $P(\rho)$ . The unperturbed state is taken close to the upper (low-density) unstable state with infinite compressibility ( $dP/d\rho = 0$ ). The evolution is shown to proceed in three different stages. At first stage, pressure and density set in the equilibrium equation of state, and velocity profile steepens gradually as in case of pressure-free flows. At second stage, those regions of the flow where anomalous pressure (*i.e.*, with negative compressibility) holds, create velocity profile more sharp than in pressure-free case, which in turn results in formation of a very narrow (short-wavelength) region where gas separates the equilibrium equation of state and pressure equilibrium sets in rapidly. On this stage, variation in pressure between narrow dense region and extended environment does not exceed more than 0.01 of the unperturbed value. On third stage, gas in the short-wavelength region reaches the second (high-density) stable state, and pressure balance establishes through the flow with pressure equal to the one in the unperturbed state. In external (long-wavelength) regions, gas forms slow isobaric inflow toward the short-wavelength layer. The duration of these stages decreases when the ratio of the acoustic time to the radiative cooling time increases. Limits in which nonlinear evolution of thermally unstable long-wavelength perturbations develops in isobaric regime are obtained.

47.70.Mc, 95.30.Qd

## I. INTRODUCTION

Thermal instability is thought to be a mechanism which causes a radiatively cooling medium (RCM) to break onto two phases: relatively dense cold filaments and clumps surrounded by rare hot plasma. This phenomenon is common for both cosmic and laboratory optically thin plasmas which lose their energy radiatively (see for more discussion [1]). A comprehensive linear theory of thermal instability has been developed in the pioneering paper by Field [2]. The instability results from the fact that the radiative energy loss rate grows with density. A local increase of the density brought in a uniform equilibrium plasma, enhances cooling rate and stimulate temperature to fall. This leads in turn to subsequent progressive growth of the density in order to keep pressure constant.

Last decade, nonlinear aspects of thermal instability have been extensively investigated both analytically and numerically, and considerable progress in understanding of the dynamics of phase transitions and structure formation in bistable media was achieved.

The equations governing dynamics of RCM, besides the nonlinearities intrinsically connected with gas dynamics processes, contain also nonlinearities related to radiative energy loss rate,  $\dot{E}(\rho, T)$ , which is square function of density and, as a rule, strongly nonlinear function of temperature. In general, nonlinear dynamics of such media is complex for analytical study, and several approximations were used to reduce the equations to more simple and useful form. This procedure is based on the presence of different characteristic time scales in RCM: characteristic radiative cooling time  $\tau_R$ , conductive time  $\tau_\chi$ , and acoustic time  $\tau_A$ . When these times differ considerably from each other one can find the fastest process which relaxes to its equilibrium state, and thus eliminate one of the governing equations. In this manner Doroshkevich and Zeldovich [3], assuming the medium to follow isobaric dynamical regime, have described dynamics of RCM by a nonlinear heat-diffusion equation

$$\frac{\partial T}{\partial t} = \frac{\partial}{\partial q} \chi(T) \frac{\partial T}{\partial q} - \varepsilon(T),$$

which belongs to a class of diffusion-reaction equations, here the reduced cooling function  $\varepsilon(T)$  represents the “reaction” term. In subsequent papers Meerson and Sasorov [4], and then Meerson *et al.* [5] have developed this approach to reduce the dynamics of RCM to more simple set of equations depending on interrelation between characteristic times. In the short-wavelength limit when acoustic time is the shortest, the dynamical regime is isobaric and the equations of motions are reduced to a diffusion-reaction equation in Lagrangian variables [5], and contrary, when acoustic time is the longest (the long-wavelength limit), the dynamics of RCM is described by equations of gas dynamics with equation of state determined by “thermal equilibrium”, *i.e.*, by balance between radiative cooling and external heating [4].

The above approximations suggest that the wavelength of perturbations of hydrodynamical variables satisfies one of the two strong inequalities:  $\tau_A \ll \tau_R$  for the short-wavelength and  $\tau_A \gg \tau_R$  for the long-wavelength limits, respectively. Perturbations with wavelengths close to the characteristic length, *i.e.*,  $\tau_A \lesssim \tau_R$  or  $\tau_A \gtrsim \tau_R$ , show complex behavior and require in general numerical study treated with the full set of equations. We address in this paper the question of what are the wavelength limits in which isobarical approximation can be used for description of thermal instability. We consider perturbations which initially are small (*i.e.*, linear), and show that these limits are rather broad: at  $t > 3 - 15 \tau_A$ , perturbations with wavelengths much larger than wavelengths determined by Meerson *et al.* [5], *i.e.*,  $\tau_A \gg \tau_R$ , evolve isobarically. Our conclusion is therefore that at comparatively late stages long-wavelength perturbations can be described by a diffusion-reaction type equation for temperature and density, equivalent to the equation for isobaric short-wavelength perturbations. Initial stages of long-wavelength perturbations can be understood in terms of wave dynamics in a pressure-free medium, and are reasonably described by nonlinear advective-diffusion equation for velocity.

The paper is organized as follows: in Section II we present the basic equations and discuss limiting cases which allow analytical description, in Section III we show numerical results for long-wavelength perturbations. Section IV contains a summary.

## II. GOVERNING EQUATIONS, CHARACTERISTIC TIMES, LIMITS

### A. Equations

The basic equations governing dynamics of a radiatively cooling gas were proposed originally by Field [2] and include in the energy equation source and sink terms describing heating by external sources and radiative energy losses. In

planar geometry the equations are written as

$$\frac{\partial \rho}{\partial t} + \frac{\partial}{\partial x}(\rho u) = 0, \quad (1)$$

$$\rho \left( \frac{\partial u}{\partial t} + u \frac{\partial u}{\partial x} \right) + \frac{\partial P}{\partial x} = \eta \frac{\partial^2 u}{\partial x^2}, \quad (2)$$

$$\frac{1}{\gamma - 1} \left( \frac{\partial P}{\partial t} + u \frac{\partial P}{\partial x} \right) + \frac{\gamma}{\gamma - 1} P \frac{\partial u}{\partial x} + \rho \mathcal{L}(\rho, T) - \frac{\partial}{\partial x} \left( \chi \frac{\partial T}{\partial x} \right) - \eta \left( \frac{\partial u}{\partial x} \right)^2 = 0, \quad (3)$$

$$P - \frac{\mathcal{R}}{\mu} \rho T = 0, \quad (4)$$

where  $\mathcal{L}$  is the net cooling function defined as  $\mathcal{L}(\rho, T) = \rho \Lambda(T) - \Gamma(\rho, T)$ , with  $\Gamma$ , as a rule, weekly dependent on  $\rho$  and  $T$ , other notations have a common meaning.

### B. Characteristic times

Three characteristic time scales are relevant for description of perturbations in RCM: acoustic time  $\tau_A = \lambda/c_0$ , conductive time  $\tau_\chi = \mathcal{R}\rho\lambda^2/\mu\chi$ , and radiative cooling time  $\tau_R = \mathcal{R}T/\Lambda\mu\rho$ , here  $c_0 = \sqrt{\gamma P_0/\rho_0}$  is the adiabatic sound speed. It is obvious that

$$\tau_\chi \sim 3\lambda^2/\ell c_0,$$

where  $\ell$  is a free-path of gas particles, and thus in framework of hydrodynamical description, *i.e.*,  $\lambda \gg \ell$ ,

$$\tau_\chi = \lambda\tau_A/\ell \gg \tau_A.$$

For cooling rate per unit mass  $\rho\Lambda(T) \sim \sigma_i c_0 \Delta E n/\mu$ , where  $\sigma_i$  is the cross-section of inelastic collisions,  $\Delta E$ , the energy lost by particles in a single inelastic collision,  $n$  is the gas number density, characteristic cooling time is

$$\tau_R = \frac{\mathcal{R}T}{\epsilon \Delta E} \frac{\ell}{c_0},$$

where  $\epsilon = \sigma_i/\sigma_e < 1$ , the ratio of inelastic-to-elastic cross-sections. Since energy transferred in a single collision, as a rule, is small compared to thermal energy  $\Delta E < \mathcal{R}T$ , we get from here  $\tau_R \gg \ell/c_0$ .

### C. Limits

Therefore, three different intervals of wavelengths are relevant, see Fig. 1: short wavelengths  $\lambda_H < \lambda < \lambda_F$ , intermediate wavelengths  $\lambda_F < \lambda < \lambda_A$ , and long wavelengths  $\lambda > \lambda_A$ , here  $\lambda_F = \sqrt{\chi_0 T_0/\rho_0 \Lambda_0}$ , the Field length determined as a length where conductive heat transfer and radiative losses equate, *i.e.*,  $\tau_R = \tau_\chi$ ,  $\lambda_A = \tau_R c_0$  is the acoustic length where  $\tau_A = \tau_R$  [1], and  $\lambda_H \sim \ell$  is the wavelength at which hydrodynamical description violates. It is seen from Fig. 1 that always the interrelation between characteristic lengths  $\lambda_H < \lambda_F < \lambda_A$  is valid. From this point of view, the “direct crossover” regime [1,6] corresponding to the case of large heat conduction,  $\lambda_A \ll \lambda_F$ , is out of the hydrodynamical approximation.

The principal difference between the short and intermediate-wavelength intervals is in more efficient conductive heat transfer compared to radiative losses for short-wavelength perturbations, which leads to erasing of a monochromatic perturbation (a normal mode with fixed wavenumber  $k = 2\pi/\lambda$ , *e.g.*,  $\delta T \propto e^{ikx}$ ) with  $\lambda < \lambda_F$  (see [1,2]). A non-monochromatic localized isobaric perturbation (a wave packet of a set of normal modes, *e.g.*,  $\delta T \propto \int \delta T_k e^{ikx} dk$ ) with

characteristic size  $L < \lambda_F$  shows decrease in amplitude at initial time, which then changes to increase due to thermal instability of long-wavelength modes presenting in the perturbation [7]. Since in these intervals  $\tau_A$  is the shortest characteristic time, pressure balance sets in first over the perturbation equations reduce to the isobaric form [3,8]

$$\frac{\partial T}{\partial t} + L(T, P) - \frac{\partial}{\partial m} \left( \tilde{\chi} \frac{\partial T}{\partial m} \right) = 0, \quad (5)$$

where

$$L(T, P) = \frac{\gamma - 1}{\gamma} \frac{\mu}{\mathcal{R}} \rho \mathcal{L}$$

is the reduced cooling function,

$$\tilde{\chi} = \frac{\gamma - 1}{\gamma} \frac{\chi}{PT},$$

the reduced heat conduction coefficient,  $T dm = dx$ ,  $P = \text{const}$ .

In the long-wavelength limit, acoustic time  $\tau_A$  is much larger than characteristic radiative cooling time  $\tau_R$ , and conductive heat transfer is negligible:  $\tau_\chi \sim \lambda^2/\chi \gg \tau_A \gg \tau_R$ , see Fig. 1. In this limit the equations can be reduced to more simple form describing gaseous medium with a given (anomalous) equation of state [4]. Indeed, when  $\tau_A \gg \tau_R$  the energy balance sets in on the shortest time  $\tau_R$ , and thus temperature and pressure relax rapidly to the values determined from the equation of steady energy balance

$$\mathcal{L}(\rho, T) = 0. \quad (6)$$

Note, that Eq. (6) with cooling function  $\Lambda(T)$  shown in Fig. 2 and  $\Gamma = \text{const}$  maps  $(\Lambda, T)$  plane on  $(P, \rho)$  plane to give the equilibrium equation of state  $P = P(\rho)$  of a van der Waals type. Equilibria with temperature in the interval where  $d \ln \Lambda(T)/d \ln T < 1$  are thermally unstable, and correspond to anomalous part of the  $P(\rho)$ -curve with  $dP/d\rho < 0$  [1,2,4]. These arguments allowed Meerson and Sasorov [4] to reduce the momentum equation of RCM in the long-wavelength limit to the one with a given (“equilibrium”) equation of state  $P = P(\rho)$

$$\rho \left( \frac{\partial u}{\partial t} + u \frac{\partial u}{\partial x} \right) + \frac{\partial P}{\partial x} = \eta \frac{\partial^2 u}{\partial x^2}, \quad (7)$$

where  $P = P(\rho)$  is determined from Eq. (6). For cooling rate with  $d \ln \Lambda(T)/d \ln T > 1$  below the temperature  $T = T_L$  and above  $T = T_U$ , and  $d \ln \Lambda(T)/d \ln T < 1$  in the intermediate interval, the equation of state has a form similar to the van der Waals equation with two rising (stable) branches of the curve  $P(\rho)$  in the low density  $\rho < \rho_U$  (high temperature  $T > T_U$ ) and high density  $\rho > \rho_L$  (low temperature  $T < T_L$ ) ranges, and a falling (unstable) branch of the  $P(\rho)$ -curve in the intermediate range  $\rho_U < \rho < \rho_L$  ( $T_L < T < T_U$ ).  $N$ -shaped curves in Figures 4 and 6 show the “equilibrium” equation of state  $P(\rho)$  corresponding to Eq. (6) with the cooling function  $\Lambda(T)$  depicted in Fig. 2 (see, also [1,6]). This equation of state is commonly used for description of pattern formation in a bistable medium in the long-wavelength limit [1]. (For the interstellar medium  $T_L \sim 10^2$  K and  $T_U \sim 10^4$  K, see [9,10]).

We will mostly concentrate in this paper on the dynamics of perturbations in an RCM which is in the upper marginally stable point:  $T \sim T_U$ ,  $d \ln \Lambda/d \ln T \sim 1$ , thus even small (linear) perturbations break the initial state. In this state an RCM can be prepared, *e.g.*, by adiabatically slow decrease of the intensity of external heating source in an RCM kept at fixed pressure  $P_U$ , or adiabatically slow increase of pressure at fixed intensity of heating sources. As at the equilibrium point  $T = T_U$  the compressibility is infinite, *i.e.*,  $dP/d\rho = 0$ , small perturbations around this point evolve to form localized structures as was demonstrated by Meerson and Sasorov [4]. In the next order positive perturbations of density decrease pressure, providing anomalous (negative) compressibility

$$P(\rho) = P_U - \frac{a^2}{2} \delta \rho^2, \quad (8)$$

where  $\delta \rho = \rho - \rho_U$ , which amplifies the nonlinearity connected with the advective term in momentum equation (3). It is clear that nonlinear term in Eq. (8) does not saturate the instability, and therefore both the advective term and

anomalous negative compressibility can be stabilized only by a strong nonlinearity in the equation of state  $P(\rho)$ , which gives rise to the second stable branch. This saturated state corresponds therefore to a new state of a medium separated onto two phases. The difference between densities of two phases being in pressure equilibrium is considerable, as a rule about two orders of magnitude, and only numerical study can be applied to these strongly nonlinear saturation stages [6]. In order to study dynamics of long-wavelength localised structures in a fluid with negative compressibility Meerson and Sasorov [4] have approximated the falling branch of the equation of state as  $P(\rho) = P_U + \text{const}/\rho$ , and described the so-called unlimited instability.

Initial stages, when  $|\delta\rho| \ll \sqrt{2P_U/a^2}$ , can be described by the advective-diffusion equation

$$\rho \left( \frac{\partial u}{\partial t} + u \frac{\partial u}{\partial x} \right) = \eta \frac{\partial^2 u}{\partial x^2}. \quad (9)$$

Numerical simulations show that equation (9) gives qualitatively reasonable description of velocity profiles up to  $t \lesssim (2 - 15)\tau_A$  depending on wavelength. Within this time interval pressure varies from  $P_U$  to minimal value  $P = P_U - \Delta P_m$ , and arising pressure gradients force then velocity to steepen sharply. It forms, in turn, a short-wavelength region, where thermal regime separates the “equilibrium” equation of state  $P = P(\rho)$  and isobaric distribution sets in rapidly, and then velocity relaxes gradually to profiles adequate to isobaric dynamics. We argue therefore, that at larger times *long-wavelength* perturbations in RCM evolve isobarically, and can be described by equation (5).

### III. NUMERICAL RESULTS

To confirm this conclusion we show here two numerical models which follow the evolution of perturbations from initial linear state to final asymptotic behaviour. In numerical simulations we have used a 6-parametric finite difference scheme of Eqs. (1)–(4) which is free of nonphysical effects of numerical viscosity and absolutely stable (the detailed description of the scheme will be given elsewhere).

To make presentation more clear we use dimensionless variables with length, time and velocity normalized, respectively, to the initial size  $\lambda$  of a perturbation (which is assumed to be localized), to the dynamical time  $\tau_A = \lambda/c_0$ , and to the adiabatic sound speed  $c_0$ ; hydrodynamical variables  $\rho$ ,  $P$  and  $T$  are normalized to their unperturbed values. In these units cooling time is equal to  $\tilde{\tau}_R = \tau_R/\tau_A$ . As we concern here dynamics of long-wavelength perturbations, the characteristic size is  $\lambda > \lambda_F$ , (in numerical examples given in the paper  $\lambda_F = 0.001\lambda$ ). Dimensionless cooling function  $\Lambda(T)$  has been taken in the form

$$\Lambda(T) = \left\{ \alpha_1 + \alpha_2 \tan\left[\frac{\pi}{2}(T^* - T)\right] \right\}^{-1}, \quad (10)$$

as shown in Fig. 2. This function represents typical cooling function for bistable media, and generates equation of state of the van der Waals type when “thermal equilibrium”, *i.e.*,  $\rho\Lambda(T) = \Gamma(\rho, T)$  is reached; we assume through the paper  $\Gamma(\rho, T) = \Lambda(1) = \text{const}$ . The unperturbed state was taken near the upper unstable point. We present here results with initial conditions taken in the form of small velocity perturbations corresponding to a localized symmetric inflow to the center of a grid zone

$$u(x, 0) = \begin{cases} -u_0 \sin[k(x - x_0)], & |x - x_0| \leq 2\pi/k, \\ 0, & \text{otherwise,} \end{cases} \quad (11)$$

while perturbations of  $\rho$ ,  $T$ , and  $P$  were zero. This choice of initial conditions seems to be most appropriate in study of long-wavelength perturbations. Due to radiative losses initial conditions corresponding to perturbations of density, temperature and pressure are inevitably more affected by the procedure of preparation such perturbations. We therefore, do not consider here alternative dynamics which would start from small perturbations of density, temperature and pressure.

For adopted type of initial conditions velocity perturbations disturb density, temperature and pressure, and radiative cooling drives them to relax in a short time to values determined by thermal equilibrium (6). Arising gradients of pressure redistribute then velocities, such that the resultant velocity field tends to set the flow in isobaric regime. At late stages the flow is approximately isobaric through the perturbed region. The boundary conditions used correspond to a “closed” box, *i.e.*, zero velocity and gradients of density and pressure. In most models the grid zone size was 20 times of the size of a localized perturbation, however test runs with larger size (80 times of the perturbation)

show results to be insensitive to the grid size. This is a direct consequence of the fact that the compressibility in the unperturbed state (which is taken to be close to the upper unstable point) is very high, and a localized perturbation propagates slowly: the acoustic velocity  $c_U = \sqrt{(dP/d\rho)_U} \simeq 0.25$ . Moreover, the initial perturbation brings most fraction of perturbed gas into a state with negative compressibility where the perturbation does not propagate. The time required for perturbations to reach a boundary is therefore at least 80 dynamical times, which is larger than the total computational time in all cases we considered. This means, that the boundary conditions we used weakly affect dynamics of perturbations. (Note, that systems whose unperturbed states lie on the low-density stable branch well below the upper unstable point, can be brought into thermal instability only by perturbations of finite, *i.e.*, not small, amplitude. We do not consider such cases in this paper.)

Fig. 3 shows dynamics of a perturbation with initial amplitude of velocity  $u_0 = 0.03$  and with  $\tilde{\tau}_R = 0.33$  (*i.e.*,  $\lambda = 3\lambda_A$ ), thus it corresponds to the long-wavelength limit. On the upper panel velocity profiles are plotted. At initial times,  $t \leq 10$ , as gas in central regions is involved in motion the velocity amplitude decreases. In gases with normal equation of state, *i.e.*,  $dP/d\rho > 0$ , perturbation decays onto two acoustic waves propagating in opposite directions, and a standing and damping entropy mode [in case of perturbations given by eq. (11), decayed waves represent two pieces of sinusoidal waves with velocity amplitude of  $u_0/2$ ]. Radiative losses with  $\tilde{\tau}_R \ll 1$  modify the inflow, transferring the internal (compressed) gas onto the anomalous part of equation of state ( $dP/d\rho < 0$ ), and thus make the perturbation locally growing, *i.e.*, non-decaying. At times  $10 < t < 15$  the velocity profile steepens and motion concentrates in a rather narrow region with increasing density, as shown in the bottom panel.

Relaxation of pressure to the equilibrium (anomalous) equation of state  $P(\rho)$  occurs at times  $t \sim \tilde{\tau}_R$  (these stages are not shown). Increasing density in central regions amplifies pressure gradient through the perturbation, and thus forces the velocity amplitude to increase. It results in more sharp steepening of velocity profiles compared to the pressure-free case as seen in Fig. 3a for time interval  $10 < t < 15$ : the profile for  $t = 15$  clearly shows two inflection points outside the central region very close to peak values, which is not what can be expected for pressure-free motions, or motions with normal equation of state. In turn, the inflow with increasing velocity amplitude forms very narrow region (a “droplet” with sizes  $\Delta x \ll \lambda$ , as seen in Fig. 3b), through which pressure equilibrium sets in rapidly. As a result, at these stages structure of the perturbation can be understood as distinguished onto two regions: first, the “long-wavelength” part outside the “droplet” where the equilibrium equation of state dominates, and second, the “short-wavelength” part (the “droplet” itself) where motion tends to set in the pressure equilibrium. The two regimes manifest themselves clearly in Fig. 4, where loci  $P - \rho$  connecting pressure and density through the computational zone for different times, *i.e.*,  $P(x, t)$  and  $\rho(x, t)$  profiles with eliminated  $x$ , are plotted: the short piece of line at the upper equilibrium point shows  $P - \rho$  locus for  $t = 10$ . The locus corresponding to  $t = 15$  is readily seen to consist of two parts: a small piece of a  $P - \rho$  curve starting from the unperturbed state with decreasing pressure and density almost parallel to the *growing* branch of the equation of state (corresponding to external, long-wavelength regions of the perturbation where density and pressure decrease), which then turns around and goes with increasing density and almost constant pressure (this part corresponds to internal, short-wavelength regions). Thus, at these stages pressure *separates* the equilibrium curve  $P(\rho)$ , and subsequent evolution is characterized by settling the overall flow down to isobaric regime. At  $t \gtrsim 20$  most fraction of density perturbation concentrates in the isobaric “droplet” with characteristic size of  $|x - x_0| = 0.2$  and in the conductive interface, which are in pressure equilibrium with gas outside (variation in pressure through the perturbed region is less than 0.001, and main contribution comes from surrounding regions where density and pressure lie on the equilibrium equation of state). (Strongly speaking, in models with “closed” box boundary conditions we used, pressure depends on time. However, as mentioned above, in all considered cases asymptotic behaviour of perturbations establishes on time interval shorter than the time required for a perturbation to reach boundaries. One can think, therefore, that isobaric regimes asymptotically established in numerical models with “closed” box boundaries give qualitatively correct description of the situation in systems with free boundary and fixed external pressure.)

After the short-wavelength droplet is formed, velocity decreases to  $u < 0.01$  with profiles corresponding to a weak inflow, so more gas continues to increase mass of the droplet. Subsequent evolution follows the isobaric regime with  $P - \rho$  loci practically coincident with that reached at  $t = 20$ , as shown in Fig. 4. Note that in models with fixed equilibrium equation of state  $P = P(\rho)$ , see [1,6], the established inflow velocity is, in general, higher than in our calculations with energy equation (3) solved explicitly. This is due to the fact that in models with the equilibrium equation of state,  $P = P(\rho)$ , pressure reaches minimal value in the interface layer, and thus at equal conditions (*e.g.*, viscosity and conductivity) arised pressure gradients generate higher acceleration.

In Fig. 5 and 6 we show results for a perturbation with larger spatial size:  $\lambda = 30\lambda_A$ , *i.e.*,  $\tilde{\tau}_R = 0.033$ . Initial conditions are same as in the previous case. The perturbation is seen to reveal similar behavior as that of smaller size, however, the dynamics is more violent. The difference is mainly in time scales and the amplitude of velocity: perturbations of longer wavelength develop higher velocities and pass same stages quicker. The enhanced steepening of the velocity profile due to negative compressibility occurs at  $t \lesssim 2$ . Here the difference between enhanced and

normal steepening is more obvious than in previous case: rather flat increase in velocity in outer regions, and very sharp growth near the symmetry plane. At  $t \sim 3$  the inflow with amplitude  $u \simeq 0.08$  forms a narrow short-wavelength droplet with almost constant pressure inside [as seen from  $P - \rho$  loci on  $(P, \rho)$  plane, Fig. 6]. However, as the velocity amplitude developed is large, pressure in the droplet is higher than the unperturbed value by  $\Delta P \sim \rho u^2 \sim 0.01$ , and in very central parts of the droplet overpressure reaches the value  $\Delta P \sim 0.03$  due to higher densities [note, that  $P - \rho$  locus in the central overpressured region goes along the equilibrium equation of state  $P(\rho)$  corresponding to the second stable brach]. On next stages,  $3 < t \lesssim 4$ , the overpressure leads to expansion of the short-wavelength region (with almost isobaric pressure distribution inside) to relax to the equilibrium with external regions. This relaxation occurs more violent than in the previous case, due to larger variations in pressure,  $|\Delta P| \sim 0.01 - 0.03$  around the unperturbed state. As a result, subsequent growth of gas mass in the short-wavelength (droplet) region proceeds in a damped oscillatory regime, as seen on  $(P, \rho)$  plane in Fig. 6.

The dependence of dynamics of perturbations on wavelength (or equivalently on  $\tau_R$ ) can be understood qualitatively from simple estimations of steepening of velocity profiles. The characteristic formation time of a short-wavelength region (a droplet) due to steepening can be estimated from  $at_d^2 \sim 2\lambda$ , where  $a$  is the acceleration caused by the negative compressibility,

$$a \sim \frac{|\nabla P_m|}{\rho_0} \sim \frac{\Delta P_m}{\rho_0 \lambda}, \quad (12)$$

$\Delta P_m$  is the maximal deviation of pressure from the unperturbed value due to density increase. This gives in dimensionless units

$$t_d \sim \sqrt{\frac{2}{\Delta P_m}}. \quad (13)$$

The deviation of pressure from the unperturbed value increases along the equilibrium  $P(\rho)$ -curve until radiative cooling time  $\tau_R$  is less than the acoustic time for the shortest wavelength  $\lambda_s$  generated due to steepening. Thus,  $\Delta P_m$  can be determined from the condition  $\tilde{\tau}_R = \lambda_s$ . To estimate  $\lambda_s$  we assume that perturbation of density caused by initial inflow (11) in dimensionless units is  $\delta\rho_0(x) \sim u_0(x)$ . Then, due to thermal instability it grows as  $\delta\rho(x, t) \sim u_0 \exp(t/\tau_R)$ . On the other hand, one can expect that  $\lambda_s \sim \lambda \exp(-t/\tau_R)$ , thus giving  $\delta\rho \sim u_0/\lambda_s$ . Substituting here  $\Delta P_m \sim c_A^2 \delta\rho$ , where  $c_A^2 = |dP/d\rho|$  estimated on the anomalous branch of equation of state [ $c_A^2 \sim 0.1$  at  $\rho \sim 1.5$ ]

$$\Delta P_m = \frac{u_0 c_A^2}{\lambda_s}, \quad (14)$$

We obtain therefore for  $t_d$ :

$$t_d \sim \sqrt{\frac{2\tilde{\tau}_R}{u_0 c_A^2}}, \quad (15)$$

which provides with reasonable accuracy an estimate for the time when the numerical solutions turn from the regime with the equilibrium equation of state,  $P(\rho)$ , to the isobaric regime.

It is clear from these estimates and from numerical results presented, that at small values of the ratio  $u_0 c_A^2 / \tilde{\tau}_R$  (less than 0.1) long-wavelength perturbations develop quiescently as isobaric. In dimensional units the condition for long-wavelength perturbations to evolve in a quiescent isobaric regime is written as

$$\frac{\tau_A}{\tau_R} \lesssim 0.1 \frac{c_0}{u_0} \left( \frac{c_0}{c_A} \right)^2. \quad (16)$$

When  $u_0 c_A^2 / \tilde{\tau}_R > 0.1$ , high pressure gradients developed at initial “equilibrium” stages [*i.e.*, along  $P(\rho)$  equation of state] give rise to very fast steepening of velocity profiles, and as a result to formation of the overdense and overpressured central short-wavelength droplet, which then relaxes to the equilibrium in an oscillatory regime with variations in pressure of  $|\Delta P| \lesssim 0.03$  around the unperturbed value. Regimes with the equilibrium equation of state,  $P(\rho)$ , can exist for long-wavelength perturbations only at initial stages,  $t \lesssim t_d$ . Subsequent evolution implies generation

of a short-wavelength core, which in turn results in separation of pressure of the equilibrium curve  $P(\rho)$ . Formation of such a short-wavelength region is an inevitable consequence of the “unlimited” instability when narrow localized structure develops in a medium on the anomalous branch of the equilibrium equation of state<sup>4</sup>. In Fig. 7 we show the dependence of pressure in the central droplet on time for several values of  $\tilde{\tau}_R$  and fixed  $c_A^2 = 0.1$  at  $\rho = 1.5$ . The amplitude of pressure oscillations is clearly seen to increase for smaller  $\tilde{\tau}_R$ : approximately, at initial times, when the central droplet follows the equilibrium equation of state,  $\Delta P_0 \sim \Delta P_m \sim u_0 c_A^2 / \tilde{\tau}_R$ . The period of oscillations is  $\mathcal{T} \sim \lambda_s \sqrt{\rho_d / \Delta P}$ , where  $\rho_d = 5$  is the density on the second stable branch; at initial times  $\mathcal{T} \sim 2.24 \tilde{\tau}_R^{3/2} / \sqrt{u_0 c_A^2}$ , however then it grows due to damping of  $\Delta P$ .

#### IV. SUMMARY

We have considered nonlinear evolution of initially small (linear) perturbations in a radiatively cooling medium in the long-wavelength limit, *i.e.*, when acoustic time is larger than radiative cooling time. We have not been assuming pressure and density to satisfy the equilibrium equation of state, but studied the problem numerically with the radiative energy loss term in energy equation treated explicitly. For initial conditions in the form of small localized velocity perturbation around a uniform equilibrium close to the upper unstable point, we have shown that early stages of evolution tend to proceed along the equilibrium equation of state,  $P(\rho)$ , with velocity profiles to steepen as in pressure-free case. At intermediate stages density increases enough and anomalous (negative) compressibility becomes important and results in more sharp steepening of velocity profiles, which in turn forms a narrow (short-wavelength) region where pressure separates the value determined by the equilibrium equation of state and sets in approximate isobaric distribution rapidly. One may say that thermal instability works as a regulator which prevents large pressure gradient to arise. The maximal amplitude of pressure developed in the perturbation when it separates the equilibrium curve  $P(\rho)$ , is proportional to the amplitude of initial velocity perturbation and inversely proportional to the radiative cooling time [as described by Eq. (14)]

$$\Delta P_m \sim P_0 \frac{u_0}{c_0} \frac{\tau_A}{\tau_R} \left( \frac{c_A}{c_0} \right)^2. \quad (17)$$

At late stages, gas in the short-wavelength region reaches the high-density (stable) equilibrium branch of the equation of state, and subsequent evolution corresponds to the isobaric inflow of low-density gas onto the high-density core (the droplet). We have shown thus, that nonlinear evolution of long-wavelength perturbations after the time interval

$$t_d \sim \frac{c_0}{c_A} \sqrt{2\tau_A \tau_R \frac{c_0}{u_0}}, \quad (18)$$

reaches quiescent isobaric regime, if the wavelength is restricted from above as

$$\lambda < 0.1 \lambda_A \frac{c_0}{u_0} \left( \frac{c_0}{c_A} \right)^2. \quad (19)$$

In these limits, long-wavelength perturbations in thermally unstable media can be described as isobaric by the reduced equation (5). Perturbations with wavelengths longer than the limit (19), after  $t = t_d$  when pressure separates the equilibrium equation of state, develop localized oscillating structures with initial pressure amplitude determined by Eq. (14) and damped then due to viscosity.

#### ACKNOWLEDGMENTS

YS acknowledges financial support from Russian Foundation of Basics Research (grant 94-02-05016-a), and from Italian Consiglio Nazionale delle Ricerche within NATO Guest Fellowship programme 1996 (Ann. No. 219.29). We acknowledge anonymous referees for critical remarks.



- 
- [1] B. Meerson, Rev. Mod. Phys. **68**, 215 (1996).
  - [2] G. B. Field, Astrophys. J. **142**, 531 (1965).
  - [3] A. G. Doroshkevich, Ya. B. Zeldovich, Zh. Eksp. Teor. Fiz. **80**, 801 (1981) [Soviet. Phys. JETP **53**, 405 (1981)].
  - [4] B. I. Meerson, P. V. Sasorov, Zh. Eksp. Teor. Fiz. **92**, 531 (1987) [Sov. Phys. JETP **65**, 300 (1987)].
  - [5] B. Meerson, E.R. Priest, and C.D.C. Steel, Geophys. Astrophys. Fluid Dyn. **71**, 243 (1993).
  - [6] B. Meerson, C.D.C. Steel, A.M. Milne, and E.R. Priest, Phys. Fluids B **5**, 3417 (1993).
  - [7] A. Ferrara, and Yu. Shchekinov, Geophys. Astrophys. Fluid Dynamics, **84**, 273 (1997)
  - [8] B. Meerson, Astrophys. J., **347**, 1012 (1989)
  - [9] L. Spitzer, Jr., *Physical Processes in the Interstellar Medium* (Wiley-Interscience, New York, 1978).
  - [10] S.A. Kaplan, and S.B. Pikelner, *Physics of the Interstellar Medium* (Nauka, Moscow, 1979).

FIG. 1. The dependence of characteristic times on wavelength. Point  $F$  corresponds to the Field length  $\lambda_F$ ,  $A$  — to the acoustic thermal length  $\lambda_A$ ,  $H$  — to the length where hydrodinamical description violates  $\lambda_H \sim \ell$ . The interval  $\lambda_H < \lambda < \lambda_F$  corresponds to the short-wavelength limit,  $\lambda_F < \lambda < \lambda_A$  — to the intermediate wavelengths, and  $\lambda_A < \lambda$  — to the long-wavelengths.

FIG. 2. The cooling function  $\Lambda(T)$  used in the paper:  $\alpha_1 = 0.915$ ,  $\alpha_2 = 0.61$ ,  $T^* = 1.11$ . The point indicates the unperturbed state; the heating rate was taken to balance energy losses in this point.

FIG. 3. Nonlinear evolution of perturbations in RCM:  $\lambda = 3\lambda_A$ ,  $\tilde{\tau}_R = 0.33$ . Upper panel (a) shows velocity profiles for the times  $t = 0, 10, 15, 20$ . The amplitude of initial velocity perturbation is  $u_0 = 0.03$ . Density, temperature and pressure have not been perturbed. Bottom panel (b) shows density profiles corresponding to the velocity profiles given on the upper panel [initial density profile  $\rho_0(x)=\text{const}$  is not shown].

FIG. 4.  $P - \rho$  loci [obtained from  $P(x, t)$  and  $\rho(x, t)$  profiles with eliminated  $x$ ] on the  $(P, \rho)$  plane, where the graph of the equilibrium equation of state  $P(\rho)$  is also plotted. The unperturbed state corresponds to a point at the  $P(\rho)$  curve left to the upper stable point. Curves for  $t = 5, 10, 15, 20, 30$  are shown. The short piece (10) of line near this point represents (splitting)  $P - \rho$  loci for times  $t = 5$  and  $10$ .

FIG. 5. Same as in Fig. 3 for  $\lambda = 30\lambda_A$ ,  $\tilde{\tau}_R = 0.0033$ ,  $u_0 = 0.03$ . Panel (a) shows velocity profiles for times  $t = 0, 2, 3, 4$ . Panel (b) shows density profiles for times  $t = 2, 3, 4$ .

FIG. 6.  $P - \rho$  loci for the case shown in Fig. 5: curves are shown for  $t = 2, 2.5, 3, 4, 4.5, 5$ .

FIG. 7.  $P_c(t)$  for several values of  $\tilde{\tau}_R$ ; plots show  $\Delta P(t) = P_c(t) - 1$ :  $\tilde{\tau}_R = 0.33$  (a),  $\tilde{\tau}_R = 0.1$  (b) and  $\tilde{\tau}_R = 0.033$  (c). At  $t < t_d$   $P_c(t)$  monotonously decreases along  $P(\rho)$  curve to minimal value, at  $t \sim t_d$  it separates  $P(\rho)$  value and grows sharply to relax then to the isobaric distribution. Time is given in units  $\tau_A$ .

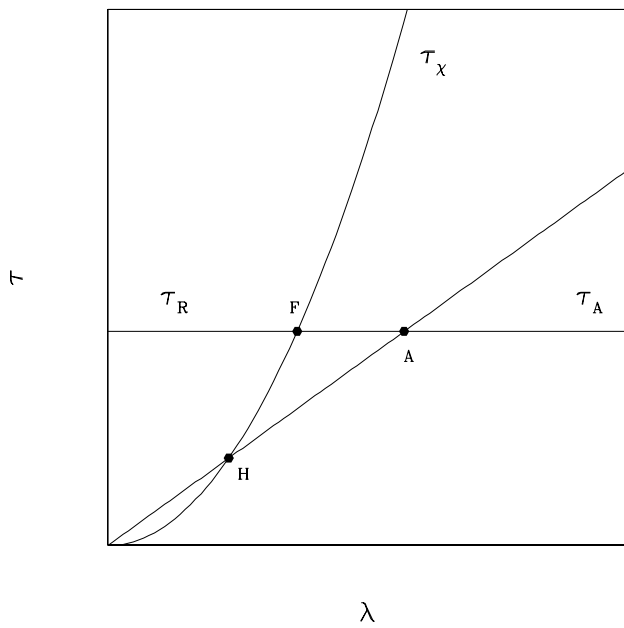


Figure 1

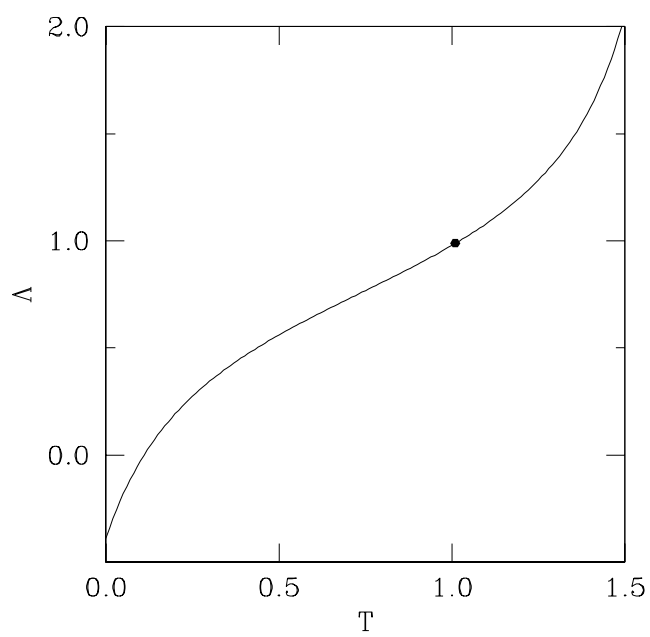


Figure 2

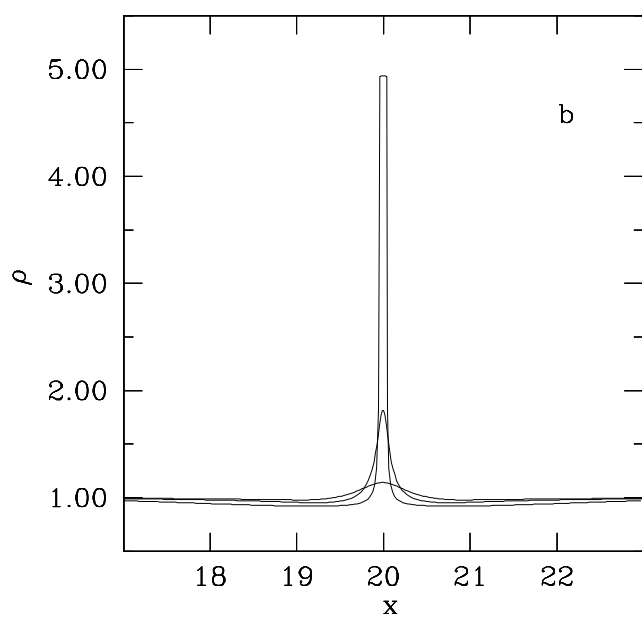
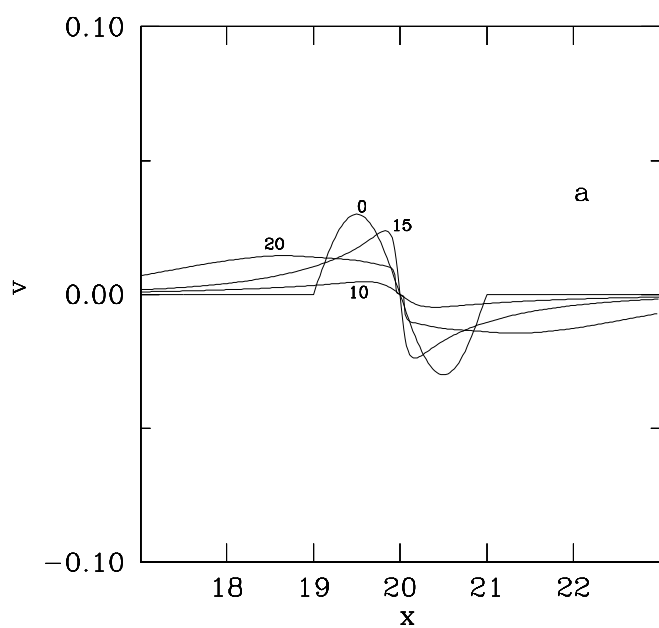


Figure 3

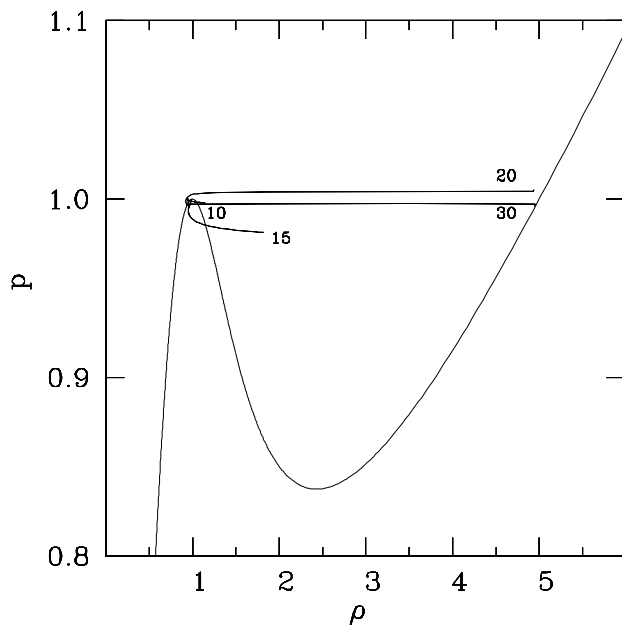


Figure 4

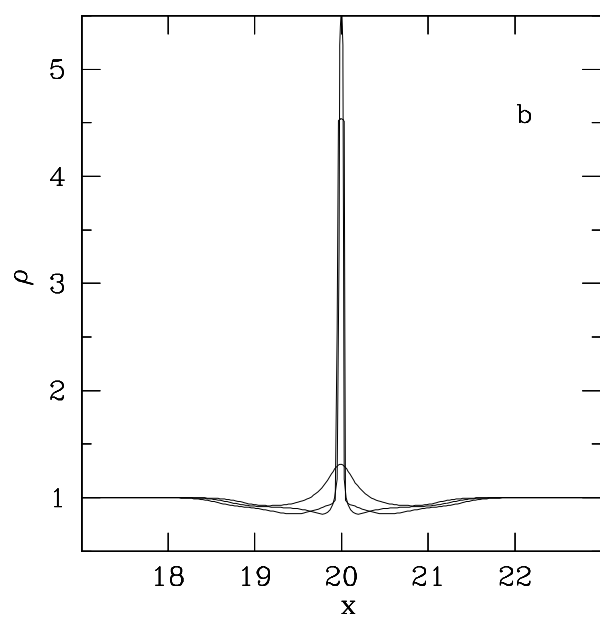
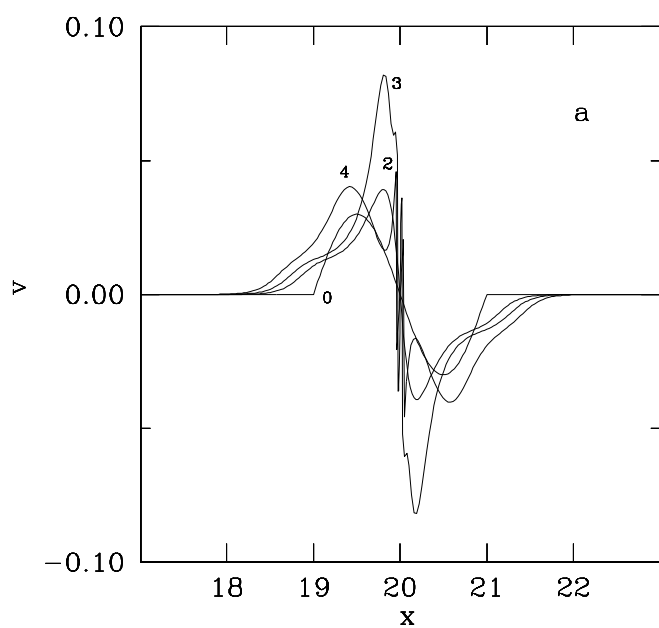


Figure 5

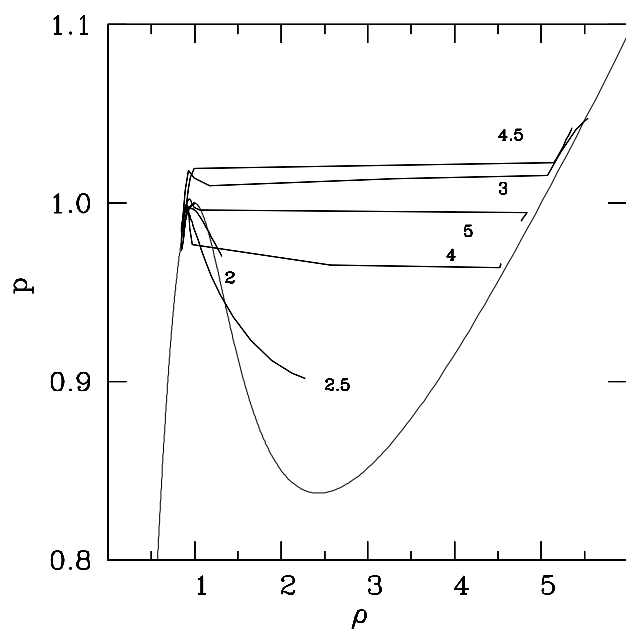


Figure 6



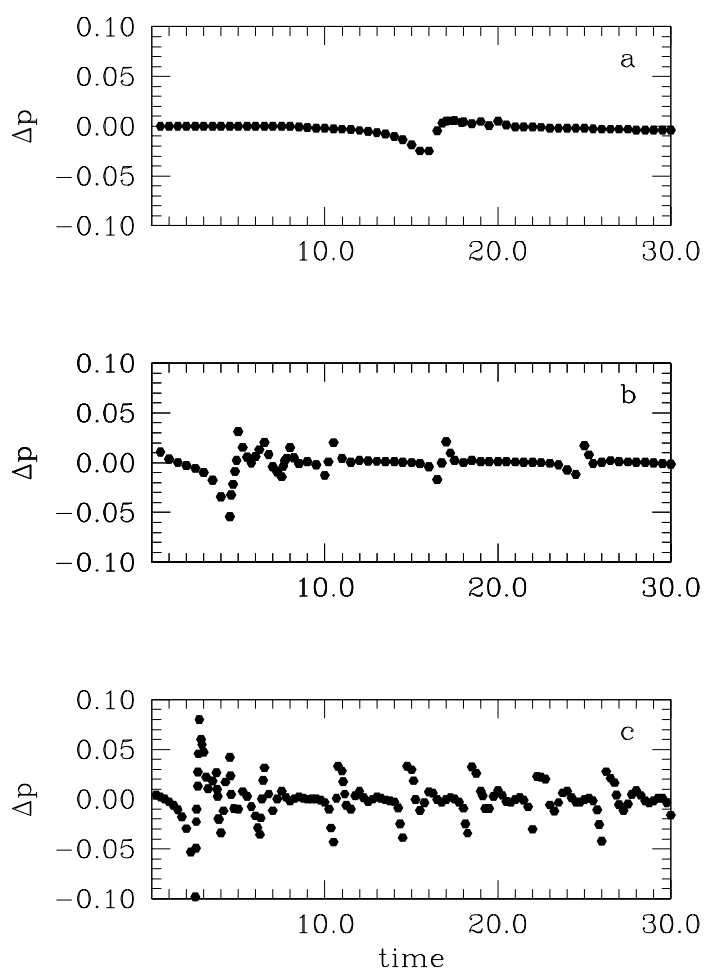


Figure 7